CLASSIFICATION OF RUBBER VULCANIZING ACCELERATORS BASED ON PARTICLE SWARM OPTIMIZATION EXTREME LEARNING MACHINE AND TERAHERTZ SPECTRA**

X. Yin [1,2*], W. He [1,2], L. Wang [1,2], W. Mo [1,2], A. Li [3]

[1] School of Electronic Engineering and Automation at Guilin University of Electronic Technology, Guangxi Guilin 541004, China; e-mail: cpxu_ck@163.com
[2] Guangxi Key Laboratory of Automatic Detecting Technology and Instruments, Guangxi Guilin 541004, China
[3] National Rubber and Rubber Products Quality Supervision and Inspection Center (Guangxi), Guilin 541004, China

In rubber tire production, three popular types of rubber vulcanizing accelerators exist that are similar in appearance (i.e., 2-Mercaptobenzothiazole, 4,4'-dithiodimorpholine, and tetramethyl thiuram monosulfide). Because the rubber vulcanizing accelerator has a great influence on the vulcanized rubber characteristics, it is necessary to classify and identify the three popular types of rubber vulcanizing accelerators to avoid using the wrong accelerator during tire production and to ensure the tire quality. The THz spectra of the accelerator samples were measured using a terahertz time-domain spectral system (THz-TDS) in a frequency range of 0.3–1.6 THz. An extreme learning machine (ELM) model was constructed to classify the three popular types of rubber vulcanizing accelerators via terahertz absorption spectra. To improve the classification accuracy of the model, a particle swarm optimization ELM model was constructed possessing a higher classification accuracy than the ELM model in the classification and identification of rubber vulcanizing accelerators.

Keywords: *terahertz spectrum, rubber vulcanization accelerator, particle swarm optimization, extreme learning machine, classification.*

КЛАССИФИКАЦИЯ УСКОРИТЕЛЕЙ ВУЛКАНИЗАЦИИ РЕЗИНЫ НА ОСНОВЕ ЭКСТРЕМАЛЬНОЙ ОБУЧАЮЩЕЙ МАШИНЫ С ОПТИМИЗАЦИЕЙ РОЯ ЧАСТИЦ И ТЕРАГЕРЦОВОГО СПЕКТРА

X. Yin [1,2*], W. He [1,2], L. Wang [1,2], W. Mo [1,2], A. Li [3]

УДК 543.42:678.4

[1] Школа электронной инженерии и автоматизации Гуйлиньского университета электронных технологий, Гуйлинь 541004, Китай; e-mail: cpxu_ck@163.com
[2] Главная лаборатория Гуанси по технологиям и приборам автоматического обнаружения, Гуанси, Гуйлинь 541004, Китай
[3] Национальный центр контроля и контроля качества резины и резиновых изделий, Гуанси, Гуйлинь 541004, Китай

(Поступила 26 ноября 2020)

Проведены классификация и идентификация схожих по внешнему виду типов ускорителей вулканизации резины: 2-меркаптобензотиазола, 4,4'-дитиодиморфолина и тетраметилтиураммоносульфида, с целью предотвращения использования неправильного ускорителя при производстве шин и обеспечения качества шин. Спектры образцов измерены с помощью терагерцовой спектральной системы во временной области (THz-TDS) в диапазоне 0.3–1.6 ТГц. Модель экстремальной обучающей

**Full text is published in JAS V. 88, No. 6 (http://springer.com/journal/10812) and in electronic version of ZhPS V. 88, No. 6 (http://www.elibrary.ru/title_about.asp?id=7318; sales@elibrary.ru).

машины (ELM) построена для классификации трех типов ускорителей вулканизации резины по спектрам терагерцового поглощения. Для повышения точности классификации построена модель с использованием ELM и оптимизации роя частиц с более высокой точностью классификации, чем ELM-модель при классификации и идентификации ускорителей вулканизации резины.

Ключевые слова: *терагерцовый спектр, ускоритель вулканизации резины, оптимизация роя частиц, модель экстремальной обучающей машины, классификация.*

Introduction. In recent years, China's rubber industry has developed rapidly and rubber products play an important role in people's daily life. Vulcanization accelerators are essential in the rubber vulcanization process, and are thus important in the production of tire rubber. To improve rubber performance, multiple types of rubber accelerators are added in the rubber vulcanization process. However, the various types of rubber vulcanization accelerators induce significant differences in the post-vulcanization performance of rubber. Using an incorrect rubber vulcanization accelerator will impact the vulcanized rubber properties and can reduce the tire rubber quality below the specifications. Therefore, a rapid and accurate method to classify and identify different types of rubber vulcanization accelerators is required.

Traditional detection methods such as thin-layer chromatography [4], gas chromatography [5], and liquid chromatography [6] are often used to identify rubber vulcanization accelerators. However, these methods are time consuming and require tedious sample preparation procedures. Alternatively, terahertz time-domain spectroscopy (THz-TDS) provides a feasible method for substance classification detection [7], avoiding these limitations. Terahertz refers to an electromagnetic wave in the frequency range of 0.1 to 10 THz, which is located between the microwave and infrared wavelengths. The THz wave has the characteristics of low photon energy and strong penetrability and can be used to obtain a "fingerprint spectrum" that can reflect the structure of a material. The latter feature is due to the fact that the molecular vibration and rotational frequencies of many materials are in the THz frequency band, and thus the THz spectra can exhibit abundant absorption characteristics. In the field of rubber detection, Peters et al. [8] used THz spectral technology to detect natural rubber, nitrile rubber, ethylene propylene rubber, neoprene rubber, and additive carbon black. Their experimental results revealed that different materials possess different THz absorption spectra and refractive index spectra. Miao Qing et al. [9] used THz spectral technology to classify and identify three types of rubbers including chloroprene rubber, nitrile rubber and ethylene propylene diene monomer rubber. Their experimental results showed that different types of rubber can be distinguished by optical parameters such as the absorption coefficient, refractive index, and absorbance.

The goal of our study was to develop a method to classify and identify three popular types of rubber vulcanizing accelerators to ensure the quality of tire rubber. In this work, we employed THz-TDS to obtain the THz spectra of 2-mercaptobenzothiazole (MBT), 4,4′-dithiodimorpholine (DTDM), and tetramethyl thiuram monosulfide (TMTM) accelerators in the range of 0.3–1.6 THz. We then used these spectra to analyze the THz absorbency of these three types of rubber vulcanization accelerators. Finally, we constructed classification models using the extreme learning machine (ELM) and particle swarm optimization ELM (PSO-ELM) methods to classify the three types of rubber vulcanizing accelerators, comparing the classification accuracy of the two methods. After multiple classifications of the test set, the average accuracy of the PSO-ELM model was 93.34% while that of the ELM model was 80.44%. The results indicate that the PSO-ELM classification model performance is superior to ELM in the classification and detection of rubber vulcanization accelerators.

ELM and PSO-ELM methods. Huang et al. [10] proposed the ELM learning algorithm based on the single-hidden layer feed-forward neural network (SLFN), which overcomes the shortcomings of traditional backpropagation neural network algorithms.

Suppose a *p*-*S*-*q* structure is used to represent a standard SLFN, where *p* is the input layer with a total of *n* neurons; *S* represents the hidden layer with a number of nodes of one; and *q* is the output layer with a total of *m* neurons. Given an activation function of $g(x)$, the input layer link weight W (representing the output layer link weight), and the hidden layer threshold of b, we can write

$$W = \begin{bmatrix} w^{11} & w^{12} & \cdots & w^{1n} \\ w^{21} & w^{21} & \cdots & w^{2n} \\ \vdots & \vdots & \ddots & \vdots \\ w^{l1} & w^{l1} & \cdots & w^{ln} \end{bmatrix}, \quad (1)$$

$$\beta = \begin{bmatrix} \beta^{11} & \beta^{12} & \cdots & \beta^{1n} \\ \beta^{21} & \beta^{21} & \cdots & \beta^{2n} \\ \vdots & \vdots & \ddots & \vdots \\ \beta^{l1} & \beta^{l1} & \cdots & \beta^{ln} \end{bmatrix}, \tag{2}$$

$$b = \begin{bmatrix} b_1 & b_2 & \cdots & b_l \end{bmatrix}^T, \tag{3}$$

For a set of training samples with a total of R samples,

$$x_i = \left[x_{i1}, x_{i2}, \cdots, x_{ip} \right]^T \in R, \tag{4}$$

$$t_i = \left[t_{i1}, t_{i2}, \cdots, t_{iq} \right]^T \in R. \tag{5}$$

Then, the output of the ELM network can be expressed as

$$T = \begin{bmatrix} t_1 & t_2 & \cdots & t_R \end{bmatrix}, \tag{6}$$

$$t_j = \begin{bmatrix} t_{1j} \\ t_{2j} \\ \vdots \\ t_{mj} \end{bmatrix} = \begin{bmatrix} \sum_{i=1}^{l} \beta_{i1} g\left(\omega_i x_j + b_i \right) \\ \sum_{i=1}^{l} \beta_{i2} g\left(\omega_i x_j + b_i \right) \\ \vdots \\ \sum_{i=1}^{l} \beta_{im} g\left(\omega_i x_j + b_i \right) \end{bmatrix}, \tag{7}$$

where $j = 1, 2, \ldots, R$.

Minimizing the error, E, of the output is similar to a least square optimization problem, and can be expressed as

$$E = \sum_{j=1}^{N} \left\| o_j - t_j \right\|. \tag{8}$$

We expect the error E to be infinitely close to zero. In the ideal case, for a standard SLFN network structure, the output is

$$f_s(x) = \sum_{i=1}^{s} \beta_i G\left(a_i x_i + b_i \right) = o_j, \quad x_i \in R, a_i \in R, \beta_i \in R, j = 1, 2, \ldots, l, \tag{9}$$

where a_i is the input connection weight of the input layer p to the ith hidden layer node, b_i is the threshold of the ith hidden layer node, β_i is the output connection weight of the ith hidden layer node to the output layer q, and $a_i x_i$ is the inner product of a_i and x_i. Expressing the equation in a matrix gives

$$\begin{bmatrix} G\left(a_1 x_1 + b_1 \right) & \cdots & G\left(a_S x_i + b_S \right) \\ \cdots & \cdots & \cdots \\ \cdots & \cdots & \cdots \\ G\left(a_1 x_L + b_1 \right) & \cdots & G\left(a_S x_L + b_S \right) \end{bmatrix}. \tag{10}$$

Generally, the excitation function $g(x)$ can be selected from "sig," "sin," "hardlim," and so on. In this experiment, we select "sig" as the excitation function.

We assume a set of training samples where

$$x_i = \left[x_{i1}, x_{i2}, \cdots, x_{ip} \right]^T \in R, \tag{11}$$

$$t_i = \left[t_{i1}, t_{i2}, \cdots, t_{iq} \right]^T \in R. \tag{12}$$

If the SLFN can approximate the set of training samples with any small error a_i, b_i, β_i, we have

$$f_s\left(x \right) = \sum_{i=1}^{s} \beta_i G\left(a_i x_i + b_i \right) = t \cdot i = 1, 2, \cdots, s. \tag{13}$$

The above formula can be simplified into

$$H\beta = T, \tag{14}$$

$$\hat{\beta} = H^{+} T, \tag{15}$$

where H^+ is the generalized inverse of the hidden-layer response H. After finding $\hat{\beta}$, the SLFN is established. For the three rubber vulcanization accelerators, the accelerator type can be inferred by an ELM classification model previously established [11]. However, this established ELM uses a random input connection weight and hidden layer threshold, and thus the classification cannot achieve a high accuracy rate and the result is unstable.

To solve this problem, the PSO algorithm was used to obtain the optimal input connection weight and ELM threshold. The PSO was proposed by Kennedy and Eberhart [12] and treats each particle as a possible solution to the problem to be solved and gives each particle a corresponding fitness value in the fitness function. Through the mutual interparticle transmission of information, the direction and distance of the particle movement are constantly adjusted to guide the particle group to a region where a solution is possible. In this process, we can find and compare possible solutions to achieve the purpose of finding the optimal solution [13]. The rate of correct classification is used as the fitness function in the optimization algorithm model, thus improving the classification accuracy and stability and establishing a neural network model with an improved classification function. The PSO-ELM classification model chart is shown in Fig. 1, where the basic steps of the algorithm are as follows:

1. Initialize the location and movement speed of the individuals in the group.
2. Determine the loss function as the threshold criterion of the fitness function.
3. After calculation, the current individual speed and position are updated.
4. Calculate the individual fitness function value again.
5. Update the individual extremum and group extremum in the particle swarm.
6. Repeat steps 3–5 to find the optimal group extremum and obtain the input connection weight and the threshold of the hidden layer.
7. Use the ELM to obtain the output connection weight and the classification result.

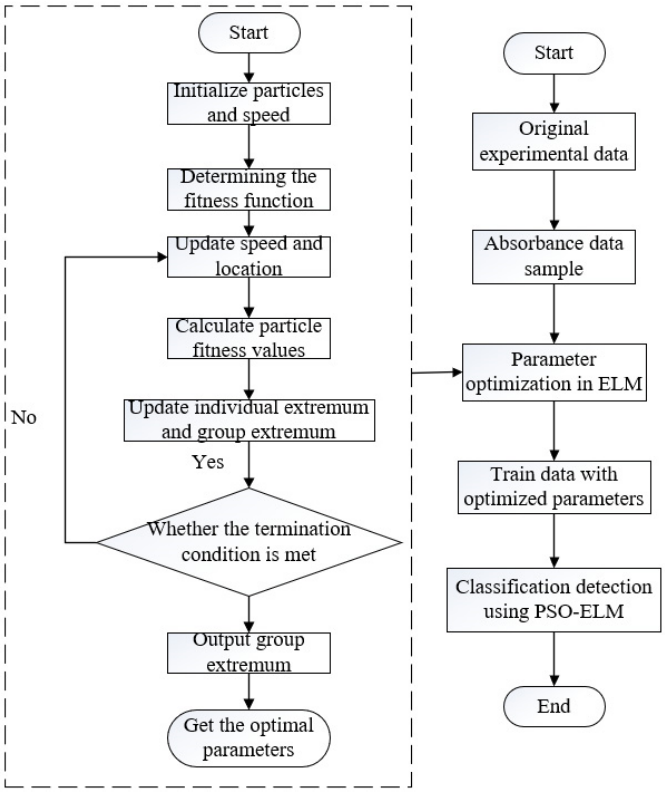

Fig. 1. Flowchart of the PSO-ELM model.

Experimental. The THz-TDS apparatus used in the experiment (Fig. 2) comprised two parts: a THz-TDS spectrometer (Z-3, Zomega Terahertz Corp., USA) and a femtosecond laser (TOPTICA Photonics Inc., Germany). The femtosecond laser generated a laser beam with a pulse width of about 100 fs, a wavelength centered around 780 nm, a repetition rate of about 80 MHz, and an average power of nearly 100 mW.

The laser beam was divided into a pump beam and a probe beam using a cubic beam splitter. The pump beam elicited a THz beam at the emitter composed of a photoconductive antenna. Then, the generated THz beam was focused onto the sample, where it interacted with the sample and left carrying the sample characteristics. The THz beam then converged with the probe beam at a zinc telluride (ZnTe) detector. After passing the detection device, the sample characteristics carried by the THz beam were loaded onto the probe beam, where the latter could also be used to measure the change of the THz beam, so that the THz waveform carrying the sample characteristics can be detected [14]. The THz-TDS used in the experiment possessed a signal-to-noise ratio greater than 70 dB and a spectral resolution exceeding 5 GHz. During the experiment, the THz-TDS apparatus was enclosed inside a box whose temperature was controlled at around 25°C. To reduce the absorption of water vapor from the ambient air, the experimental apparatus box was filled with dry air until the relative humidity within the box was less than 2%.

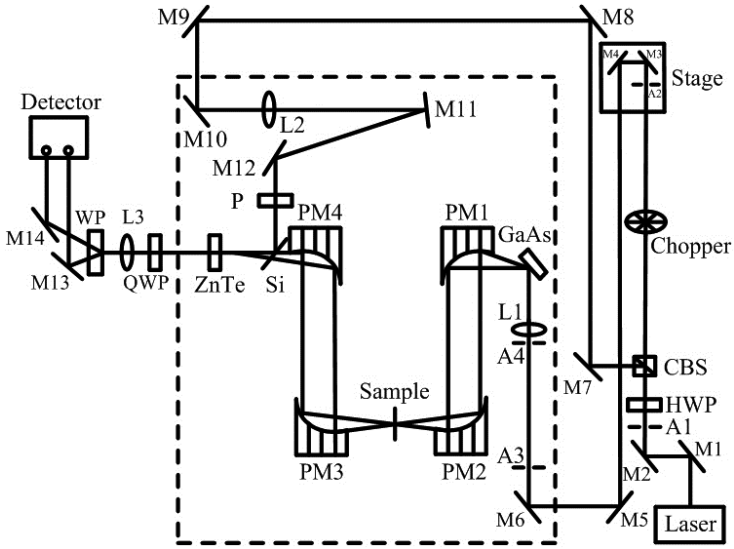

Fig. 2. Schematic of THz time-domain spectroscopy system.

Sample preparation. Samples of the three types of rubber vulcanization accelerator were purchased from the Plastic Products Company. First, to reduce the effect of air humidity on the experimental samples, all the power-form samples were placed in a YB-1A vacuum-drying oven for 2–3 h at 323 K. Second, 40 samples of the DTDM, TMTM, and MBT accelerators 180 mg in mass were weighed with an electronic balance. Finally, each powder sample was placed in a mold and pressed into a round tablet 12 mm in diameter and 1 mm thick using a tablet press, where the pressure of the tablet press was set to about 8 ton. In this way, 40 samples of each rubber vulcanization accelerator were prepared for measurements.

Data acquisition. Absorbance of the rubber vulcanization accelerator was obtained according to the parameter extraction model of the THz time-domain spectrum of Dorney and Duvillatet [15–18]. The absorbance spectrum can reflect the extent to which the experimental material absorbs THz waves. First, a THz wave transmitted through the dry air with no sample in place was used as a reference signal. Second, to avoid any influence from echoing, the time-domain waveform was truncated. Then, the time-domain spectra of the experimental samples were converted to frequency-domain spectra by fast Fourier transformation (FFT). The absorbance spectrum was acquired using [18]

$$\text{Absorbance} = -\lg[E_{\text{sam}}(\omega)^2/E_{\text{ref}}(\omega)^2], \quad (16)$$

where $E_{\text{sam}}(\omega)$ and $E_{\text{ref}}(\omega)$ are the amplitude of the sample and reference signals in the frequency domain.

Results and discussion. In the experiment, the three types of rubber vulcanization accelerators DTDM, MBT, and TMTM were selected as samples for classification and identification tests, respectively assigned corresponding digital labels of 1, 2, and 3, respectively. Forty samples of each type of vulcanization accelerator were made, and each sample was measured three times using THz-TDS. To avoid errors caused by accidental factors, an average of three scanning results was taken as the spectrum for each sample. The time-domain spectra of the three types of rubber vulcanization accelerator samples are shown in Fig. 3.

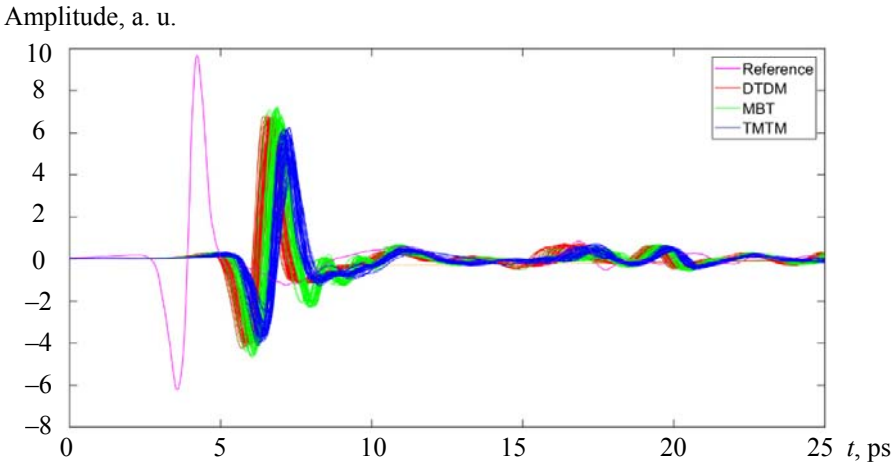

Fig. 3. Time-domain spectra.

The time-domain spectra of the three types of rubber vulcanization accelerators were converted to frequency-domain spectra by FFT, and the frequency-domain spectra are shown in Fig. 4. The three types of rubber vulcanization accelerator samples exhibit similar waveforms that rise rapidly in the range of 0–0.3 THz. Further, the waveforms exhibit a strong oscillation and multiple peaks in the range of 0.3–1.6 THz. The peak positions of the three types of vulcanization accelerator samples are similar and the peaks are difficult to distinguish. However, near 1.6 THz, the waveforms of the three types of vulcanization accelerator samples are slow and close to zero. Therefore, we selected the 0.3–1.6 THz spectral range featuring easily-distinguishable waveforms for analysis.

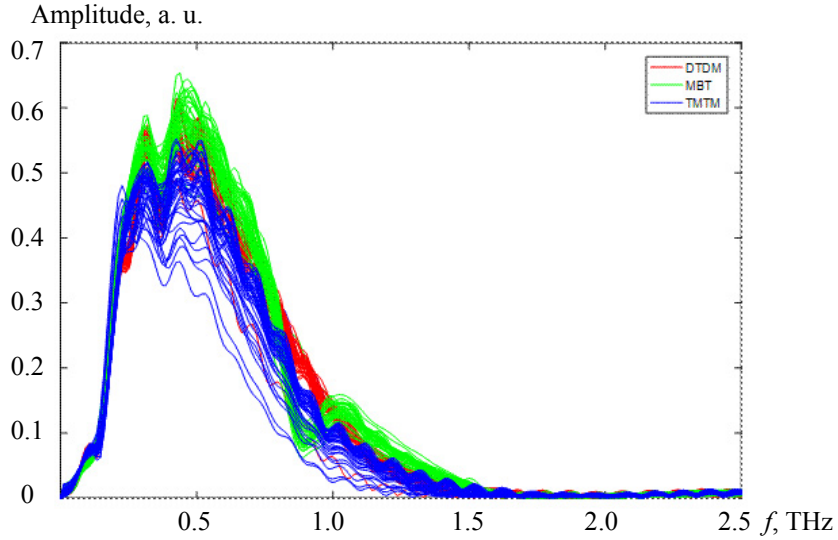

Fig. 4. Frequency-domain spectra.

Figure 5 shows the absorbance spectra of the three types of rubber vulcanization accelerator samples in this range. It can be seen from the absorbance spectra that multiple distinct absorption peaks exist in the 0.8–1.0 and 1.2–1.6 THz ranges, but the proximity of these absorption peaks makes them difficult to distinguish. Considering absorbance, the absorbance of the three sample types fluctuates significantly in different THz frequency ranges. Specifically, in the range of 0.8–1.0 THz, the MBT peak is the highest (i.e., absorbance is the strongest) while the DTDM peak is the lowest (i.e., absorbance is the weakest). In the range of 1.2–1.6 THz, DTDM has the highest peak and strongest absorbance, while MBT has the lowest peak and weakest absorbance. The difference in the characteristics and properties of the material itself is one of the primary reasons for the difference in the strength of the absorbance. Although the absorption peak positions

are close, the individuals in the same category are similar and concentrated, making it a basis for using absorbance spectra as sample data analysis.

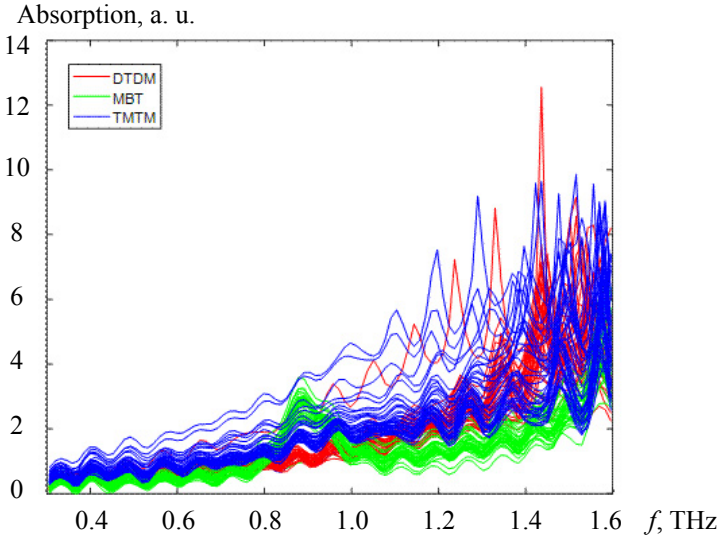

Fig. 5. Absorbance spectra.

Three types of rubber vulcanization accelerators were classified by absorbance via the ELM classification model (Fig. 6). Digital labels of one, two and three were assigned to the DTDM, MBT, and TMTM rubber vulcanization accelerators, respectively. In the 120 sets of test data, 90 sets of data were randomly selected to form the calibration set, while the remaining 30 sets of data formed the prediction set. Therefore, the prediction set for each type of vulcanization accelerator was 10 sets of data. Figure 6 plots the result of a single experiment randomly selected from the multiple classification experiments.

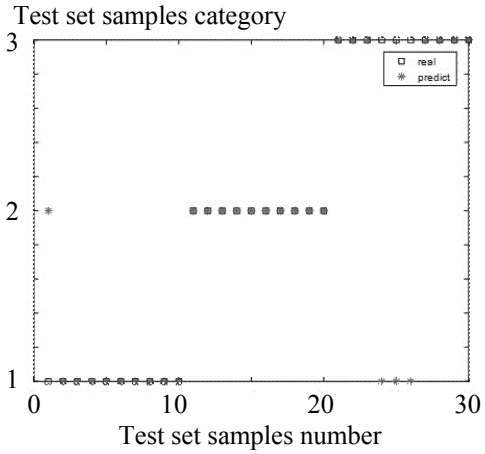

Fig. 6. Classification of ELM model prediction set.

After 50 classification experiments, the average classification accuracy of the ELM model was about 80.44%. The distribution of the 50 classification accuracy values is shown in Fig. 7. It can be seen from the experimental results that the classification accuracy of the ELM classification model is not high and the stability is poor. To improve the classification accuracy rate and the stability of the classification results, the PSO-ELM classification model was established to classify and test the three types of vulcanization accelerators. Figure 8 plots the result of classification of a single experiment randomly selected from the numerous experiments. After 50 classification experiments, the average classification accuracy rate of the PSO-ELM model was about 93.34%. The distribution of the 50 classification accuracy values is shown in Fig. 9.

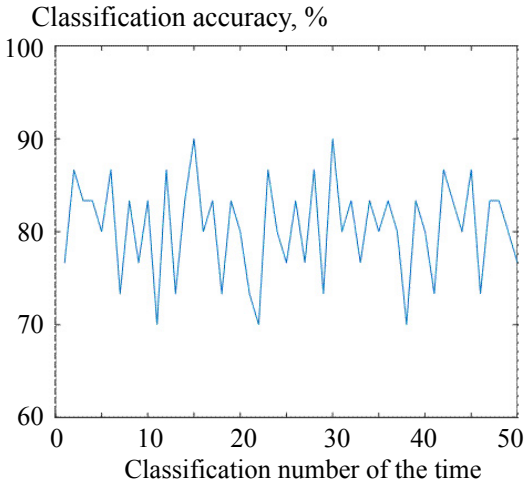

Fig. 7. ELM classification accuracy.

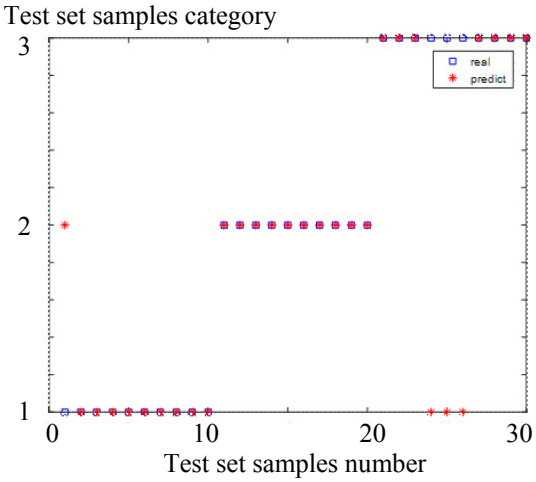

Fig. 8. Classification of the PSO-ELM model prediction set.

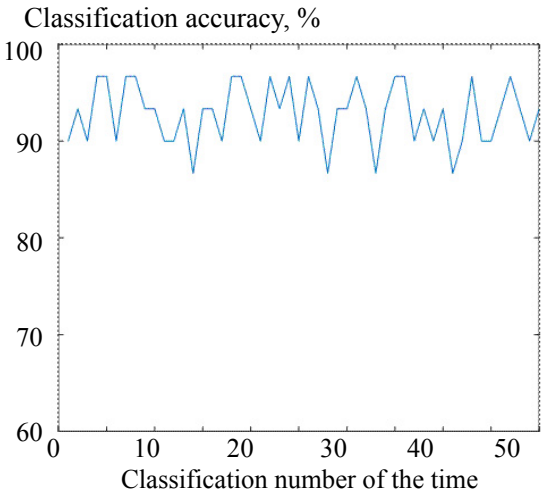

Fig. 9. PSO-ELM classification accuracy.

TABLE 1. Comparison between ELM and PSO-ELM Models

Model	Classification time, s	Classification accuracy, %	Standard deviation
ELM	0.905	80.44	5.73
PSO-ELM	2.959	93.34	3.10

A comparison of the classification effects of the two models before and after optimization is shown in Table 1 using the results of 50 experiments. As we can see from Table 1, though the ELM model has a rapid classification time, the classification accuracy rate is low and the degree of dispersion is large. Although the PSO-ELM model has a greater classification time, its classification accuracy is greatly improved and the stability is enhanced compared to the ELM model.

Conclusions. Three types of rubber vulcanization accelerators were differentiated using the THz-TDS system. The ELM and PSO-ELM classification models were established, and the average classification accuracies of the two models were compared. The average classification accuracy rate of the ELM classification model was about 80.44%, and the average classification accuracy rate of the PSO-ELM classification model was about 93.34%. It can be seen from the experimental results that the PSO-ELM classification model is superior in terms of classification accuracy and stability. The results indicate that THz-TDS detection combined with the PSO-ELM classification model is a feasible method to classify and identify rubber vulcanization accelerators quickly, stably, and accurately. It provides a new idea for THz analysis spectroscopy and gives evidence for the feasibility of classifying rubber accelerators.

Acknowledgments. This work was supported by the National Natural Science Foundation of China (NSFC) (grant No. 61841502), the Guangxi Natural Science Foundation (grant No. 2018GXNSFAA281341) and the Foundation from Guangxi Key Laboratory of Automatic Detecting Technology and Instruments (grant No. YQ19102).

We thank Sara Maccagnano-Zacher, PhD, from Liwen Bianji (Edanz) (https://www.liwenbianji.cn) for editing the language of a draft of this manuscript.

REFERENCES

1. S. H. Baek, J. H. Kang, Y. H. Hwang, K. M. Ok, K. Kwak, H. S. Chun, *J. Infrared Millimeter and Terahertz Waves*, **37**, 486–497 (2016).
2. Y. Hua, H. Zhang, *IEEE Trans. Microwave Theory Tech*., **58**, 2064–2070 (2010).
3. Z. Chen, Z. Zhang, R. Zhu, Yang, Y. Yang, P. B. Harrington, *J. Quant. Spectrosc. Radiat. Transf.*, **167**, 1–9 (2015).
4. M. Lu, T. Wang, Y. W. Wang, *Chin. Rubber Sci. Technol. Market*, **1**, 32–34 (2012).
5. F. Yan, *J. Chin. Rubber/Plastics Technol. Equip.*, **43**, No. 3, 47 (2017).
6. J. F. Rong, Sh. L. Mao, J. F. Li, *J. Phys. Test. Chem. Anal. B: Chem. Anal.*, **52**, No. 7, 750–755 (2016).
7. M. Hangyo, *Jpn. J. Appl. Phys*., **54**, 12010112 (2015).
8. O. Peters, M. Schwerdtfeger, S. Wietzke, et al., *J. Polym. Test.*, **32**, 932–936 (2013).
9. Q. Mao, L. Tian, et al., *J. Mod. Sci. Instrum*., **5**, 110–113 (2011).
10. H. B. Guang, *J. Neu-Rocomputing*, **70**, 489–501 (2006).
11. X. T. Shi, J. Y. Pang, X. Zhang, et al., *Chin. J. Sci. Instrum*., **39**, No. 12, 81–91 (2018).
12. R. C. Eberhart, J. Kennedy, *Proc. 6th Int. Symposium on Micro Machine and Human Science*, Nagoya, Japan, IEEE, 39–43 (1995).
13. Ch. P. Xu, M. Lik, *Chin. J. Sci. Instrum*., **38**, No. 3, 765–772 (2017).
14. T. Chen, Zh. Li, W. Mo, *Chin. J. Sci. Instrum*., **33**, No. 11, 2480–2486 (2012).
15. T. D. Dorney, R. G. Baraniuk, D. M. Mittleman, *J. Opt. Soc. Am. A Opt. Image SciVis*, **18**, No. 7, 1562–1571 (2001).
16. L. Duvillaret, F. Garet, J. L. Coutaz, *J. Appl. Opt*., **38**, No. 2, 409–415 (1999).
17. L. Duvillaret, F. Garet, J. L. Coutaz, *IEEE J. Sel. Top. Quantum Electron*., **2**, No. 3, 739–746 (1996).
18. H. Zhang, Z. Li, T. Chen, et al., *J. Spectrochim. Acta A: Mol. Biomol. Spectrosc*., **184**, 335–341 (2017).